Materials Transactions, Vol. 60, No. 9 (2019) pp. 1740 to 1748
Special Issue on Latest Research and Development of Structural and Functional Titanium-Based Materials

Quantitative and Qualitative Relationship between Microstructural Factors and Fatigue Lives under Load- and Strain-Controlled Conditions of Ti–5Al–2Sn–2Zr–4Cr–4Mo (Ti-17) Fabricated Using a 1500-ton Forging Simulator

M. Niinomi[1,2,3,*], T. Akahori[1], M. Nakai[4], Y. Koizumi[2], A. Chiba[3], T. Nakano[2], T. Kakeshita[5], Y. Yamabe-Mitarai[6], S. Kuroda[6], N. Motohashi[6], Y. Itsumi[7] and T. Choda[7]

[1]*Department of Materials Science and Engineering, Faculty of Science and Technology, Meijo University, Nagoya 468-8502, Japan*
[2]*Department of Materials and Manufacturing Science, Graduate School of Engineering, Osaka University, Osaka 565-0871, Japan*
[3]*Institute for Materials Research, Tohoku University, Sendai 980-5377, Japan*
[4]*Department of Mechanical Engineering, Faculty of Science and Engineering, Kindai University, Osaka 577-8502, Japan*
[5]*Faculty of Engineering, Fukui University of Technology, Fukui 910-8505, Japan*
[6]*National Institute for Materials Science (NIMS), Tsukuba 305-0047, Japan*
[7]*Kobe Steel, LTD., Kobe 675-0023, Japan*

The fatigue lives of forged Ti-17 using a 1500-ton forging simulator subjected to different solution treatments and a common aging treatment were evaluated under both load- and strain-controlled conditions: high and low cycle fatigue lives, respectively. Then, the tensile properties and microstructures were also examined. Finally, the relationships among fatigue lives and the microstructural factors and tensile properties were examined.

The microstructure after solution treatment at 1203 K, which is more than the β transus temperature, and aging treatment exhibits equiaxed prior β grains composed of fine acicular α. On the other hand, the microstructures after solution treatment at temperatures of 1063, 1123, and 1143 K, which are less than the β transus temperature, and aging treatment exhibit elongated prior β grains composed of two different microstructural feature regions, which are acicular α and fine spheroidal α phase regions. The 0.2% proof stress, $\sigma_{0.2}$, and tensile strength, σ_B, increase with increasing solution treatment temperature up to 1143 K within the $(\alpha + \beta)$ region, but decrease with further increasing solution treatment temperature to 1203 K within the β region. The elongation (EL) and reduction of area (RA) decrease with increasing solution treatment temperature, and it becomes nearly 0% corresponding to a solution treatment temperature of 1203 K. The high cycle fatigue limit increases with increasing solution treatment temperature up to 1143 K, corresponding to the $(\alpha + \beta)$ region. However, it decreases with further increase in the solution treatment temperature to 1203 K in the β region. The fatigue ratio in high cycle fatigue life region is increasing with decreasing solution treatment temperature, namely increasing the volume fraction of the primary α phase, and it relates well qualitatively with the volume fraction of the primary α phase when the solution treatment temperature is less than the β transus temperature. The low cycle fatigue life increases with decreasing solution treatment temperature, namely increasing the volume fraction of the primary α phase. The low cycle fatigue life relates well quantitatively with the tensile true strain at breaking of the specimen and the volume fraction of the primary α phase for each total strain range of low cycle fatigue testing. [doi:10.2320/matertrans.ME201904]

(Received December 25, 2018; Accepted February 19, 2019; Published April 12, 2019)

Keywords: *Ti-17, low-cycle fatigue, high-cycle fatigue, microstructure, primary α phase, solution treatment temperature*

1. Introduction

The use of titanium and titanium alloys for commercial aircrafts is recently rapidly increases because they exhibit excellent consistency with CFRP (carbon fiber reinforced plastics), which is used for air frame structures.[1)] However, titanium alloys are used not only in air frames, but also in jet engine components such as fans and compressor disks, which function at relatively low temperatures up to 673 K. Ti–5Al–2Sn–2Zr–4Cr–4Mo (Ti-17), which is an age-hardenable β-rich two-phase $(\alpha + \beta)$-titanium alloy, was developed to reduce the titanium components in the early 1970s in the USA and registered as AMS 4955; it exhibits greater strength, fatigue endurance including fatigue strength and crack propagation resistance, and creep resistance compared with those of Ti–6Al–4V at intermediate temperatures, and Ti-17 is β-forged to achieve high fracture toughness.[2–4)] Notably, fatigue endurance is one of the important factors for the aforementioned engine components.[5,6)] Investigation of the fatigue properties of Ti-17 by focusing on their relation with microstructural factors is highly significant. In particular, it is important to consider the quantitative relationship between fatigue properties and microstructural factors during the fatigue life estimation of engine components made of Ti-17. Therefore, in this study, the fatigue properties and microstructures of hot-forged disk-like Ti-17 samples were investigated to define the qualitative and quantitative relationship between the fatigue properties and the microstructural factors. Fatigue properties and other mechanical properties of Ti-17 were investigated at room temperature in this study because it is used at relatively low temperature and after subjecting aging treatment at a temperature higher than that for practical applications leading to almost no change in the microstructure.

2. Experimental

Disk-like Ti-17 samples were fabricated using a 1500-ton forging simulator.[7)] Its chemical compositions are shown in Table 1. First, a Ti-17 ingot with a diameter of 120 mm and a height of 240 mm was forged at 1073 K to a round disk-like sample. Then, a quarter of the forged disk-like sample was cut to prepare the tensile and fatigue specimens. For the preparation, the cut pieces were subjected to solution treatment (ST) at four different temperatures: 1063, 1123,

*Emeritus Professor, Tohoku University. Corresponding author, E-mail: niinomi@imr.tohoku.ac.jp

Table 1 Chemical composition of Ti-17 in mass%.

Alloy	Chemical composition (mass%)							
	Al	Sn	Zr	Mo	Cr	Fe	O	Ti
Ti-17	5.09	2.04	2.01	3.88	3.83	0.48	0.105	bal.

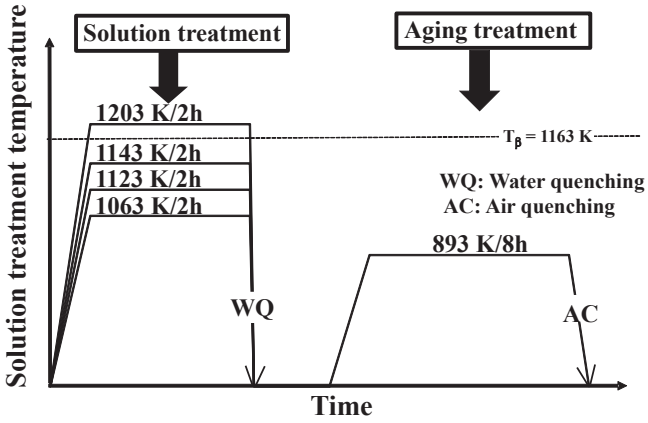

Fig. 1 Schematic illustration of heat treatment process.

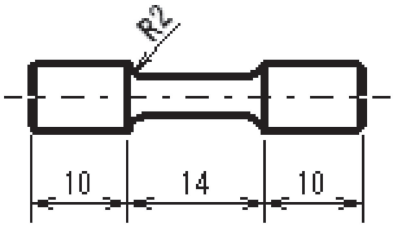

(a) Tensile test specimen

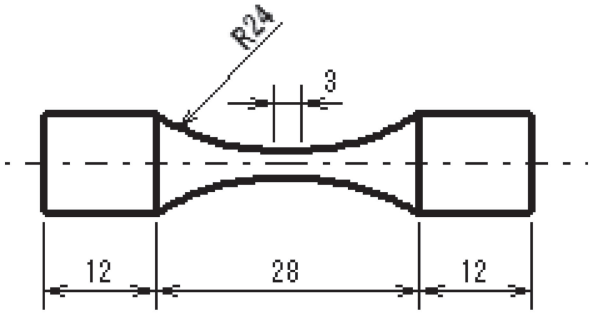

(b) Load-controlled fatigue test specimen

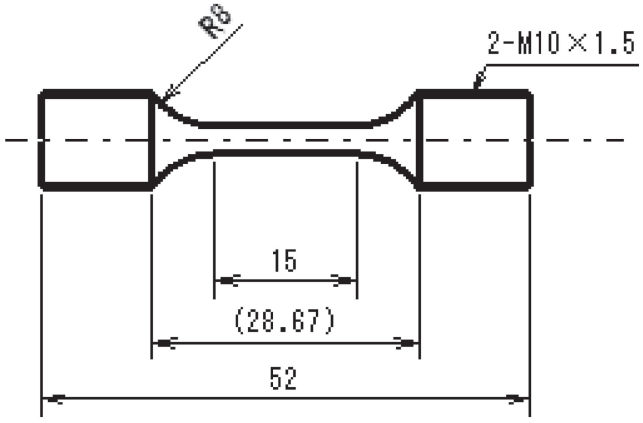

(c) Strain-controlled fatigue test specimen

Fig. 2 Geometries of (a) tensile test specimen, (b) load-controlled fatigue test specimen, and (c) strain-controlled fatigue test specimen.

1143, and 1203 K followed by water quenching (WQ). The β transus temperature of Ti-17 is approximately 1163 K; therefore, the ST temperature of 1203 K was slightly higher than the β transus temperature, but within the β region. The other three ST temperatures were lower than the β transus temperature, and in the ($\alpha + \beta$) region. Each sample was then subjected to an aging treatment at 893 K for 8 h, followed by air cooling (AC). The heat treatment processes are schematically shown in Fig. 1. The samples subjected to aging after the different STs were denoted as ST/1063 K, ST/1123 K, ST/1143 K, and ST/1203 K, according to the ST temperatures. Smooth round bar-shaped tensile specimens with a gage diameter of 7.0 mm, a gage length of 14 mm, and a total length of 34 mm, hour-glass shaped fatigue specimens with a minimum diameter of 3 mm and a length (without the gripping part) of 28 mm, and a total length of 52 mm for load-controlled fatigue tests to obtain high cycle fatigue life, and smooth round bar fatigue specimens with a diameter of 3 mm, a gage length of 15 mm, and a total length of 52 mm for strain-controlled fatigue tests to obtain low cycle fatigue life were machined from the aged samples. The specimen surfaces of tensile, and load- and strain-controlled fatigue test specimens (the geometries are shown in Fig. 2) were finished by #1500 grid SiC emery paper, mirror polishing, and #1500 grid SiC emery paper, respectively. The long axes, namely stress axes of the tensile, and load- and strain-controlled fatigue test specimens were perpendicular to the radial direction of the forged disk-like sample. Tensile tests were carried out at a strain rate of 0.5%/min up to a strain of 5% and after that, a strain rate of 1.5%/min using an Instron-type testing machine with a capacity of 10 kN, at ambient temperature. Fatigue tests under load-controlled conditions were carried out at a stress ratio of 0.1 and a frequency of 10 Hz using an electro-hydraulic servo fatigue-testing machine with a capacity of 5 kN, at ambient temperature. The maximum cyclic stress, at which the specimen did not fail at 10^6 cycles, namely fatigue strength at 10^6 cycles was defined as the fatigue limit in this study. One of the reason to investigate the fatigue strength 10^6 cycles is that the strain-controlled fatigue life is generally emphasized in aircraft engine components. The Fatigue tests under strain-controlled conditions were carried out at representatively selected total strain ranges of 1.05, 1.1, and 1.2, respectively to examine relative fatigue life among specimens using an electro-hydraulic servo fatigue testing machine with a capacity of 100 kN, at ambient temperature.

Tensile and fatigue fracture surfaces were observed using a scanning electron microscopy (SEM) at an accelerating voltage of 20 kV.

Specimens with a thickness of 4 mm for micro-Vickers hardness measurement were cut from the center of the gripping parts of the tensile tested specimens, and then finished by #1500 grid SiC emery paper. The micro-Vickers hardness of the samples was measured using a micro-Vickers

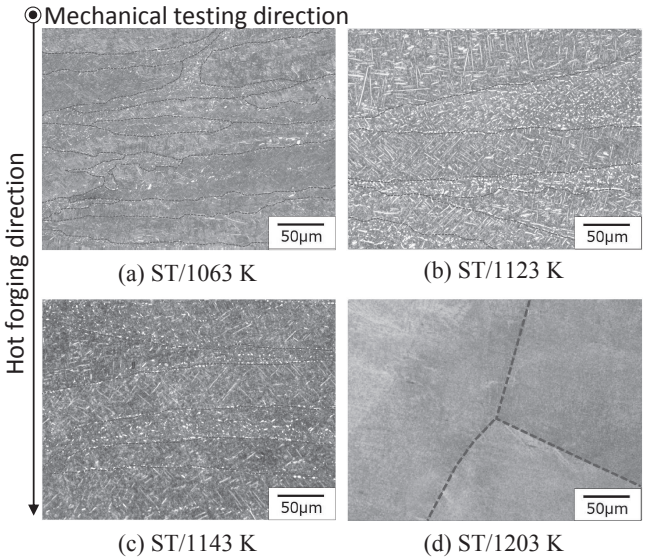

Fig. 3 Optical micrographs of (a) ST/1063 K, (b) ST/1123 K, (c) ST/1143 K, and (d) ST/1203 K.

hardness tester with an indention load of 0.245 N and a holding time of 10 s.

Specimens with a thickness of 4 mm for microstructural observations were cut from the center of the gripping parts of the tensile tested specimens, and then finished by #4000 grid SiC emery paper and buff polishing. Microstructural observations were carried out using an optical microscopy.

3. Results and Discussion

3.1 Microstructure

The optical microstructures of ST/1063 K, ST/1123 K, ST/1143 K, and ST/1203 K are shown in Fig. 3. The dotted line in each micrograph indicates the prior β grain boundary.

Table 2 Average thickness of elongated prior β grain.

Grain size	Specimen		
	ST/1063 K	ST/1123 K	ST/1143 K
Average thickness of elongated prior β grain (μm)	25.0	37.8	44.2

The microstructure of ST/1203 K exhibits equiaxted prior β grains with an average grain diameter of 546 μm composed of fine acicular α precipitated by aging treatment: secondary α because it was subjected to ST at a temperature higher than the β transus temperature. However, the microstructures of ST/1063 K, ST/1123 K, and ST/1143 K exhibits elongated prior β grains composed of two different microstructural feature regions: acicular and fine spheroidal α phase regions, both of which are primary α. The area except these primary α area is composed of secondary α and β phases. The average thickness of the prior β grain increases with increasing ST temperature as listed in Table 2.

The highly magnified optical micrographs of acicular and fine spheroidal α phase regions in ST/1063 K, ST/1123 K, and ST/1143 K are shown in Fig. 4. The volume fractions of both acicular and fine spheroidal α phases decreases with increasing ST temperature, and are listed in Table 3 with ST temperature. On the other hand, the volume fraction of (secondary $\alpha + \beta$) area increasing with increasing ST temperature: namely the volume fraction of secondary α increasing with ST temperature.

The aspect ratios (short axis divided by long axis) of acicular and fine spheroidal α phases versus their numbers in ST/1063 K, ST/1123 K, and ST/1143 K are shown in Figs. 5, 6, and 7. The number of the fine spheroidal α phase with low aspect ratio is also large, as well as that of the

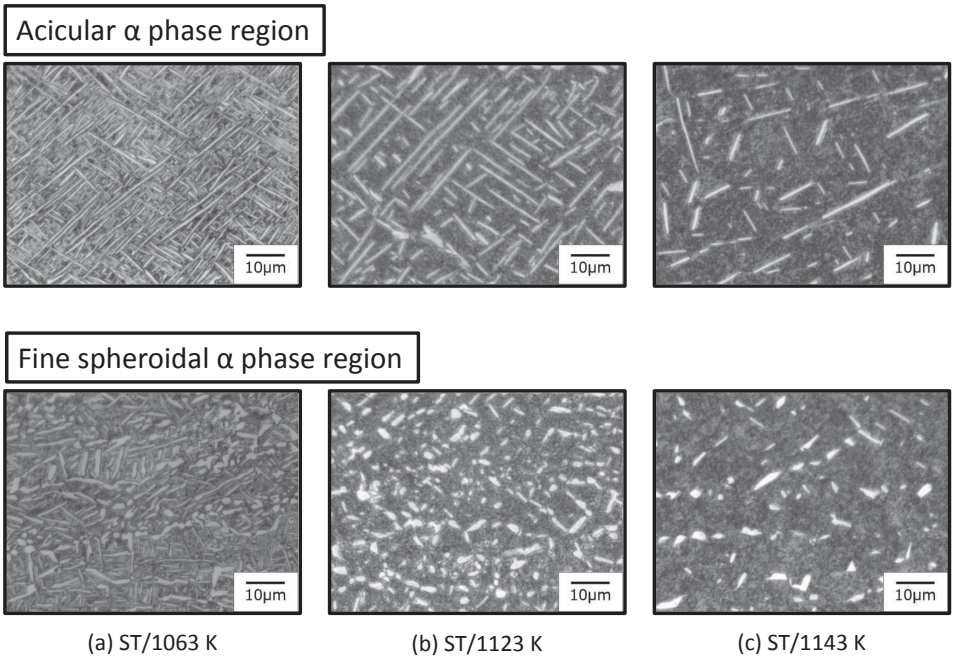

Fig. 4 Highly magnified optical micrographs of acicular and fine spheroidal α phase regions in (a) ST/1063 K, (b) ST/1123 K, and (c) ST/1143 K.

Table 3 Volume fractions of acicular and fine spheroidal α phases.

Volume fraction (%)	Specimen		
	ST/1063 K	ST/1123 K	ST/1143 K
Acicular α phase	50	24	6.1
Fine spheroidal α phase	47	22	6.3

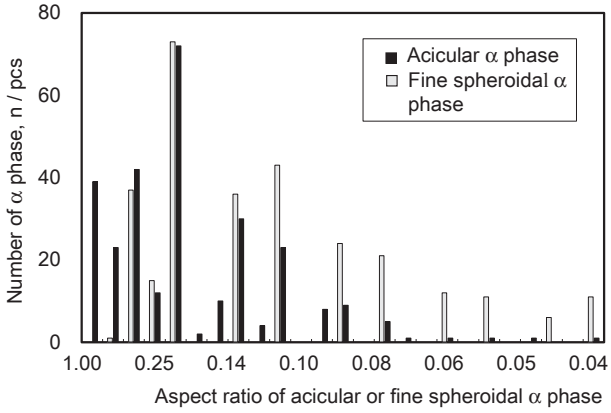

Fig. 5 Aspect ratios of acicular and fine spheroidal α phases in ST/1063 K.

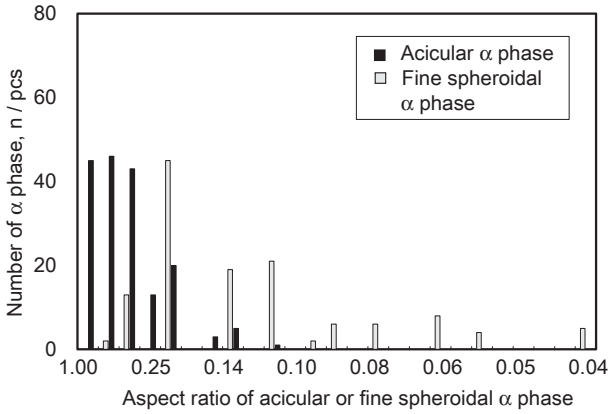

Fig. 6 Aspect ratios of acicular and fine spheroidal α phases in ST/1123 K.

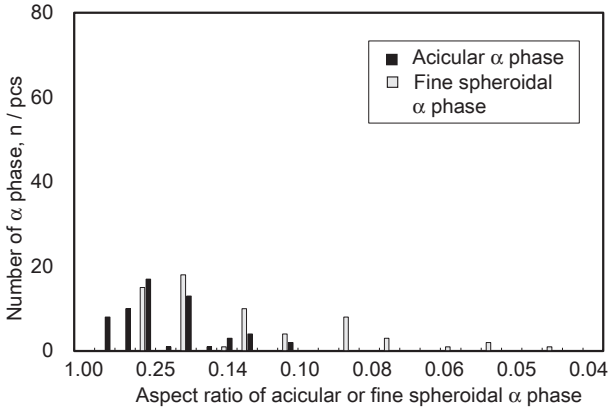

Fig. 7 Aspect ratios of acicular and fine spheroidal α phases in ST/1143 K.

acicular α phase at the lowest ST temperature of 1063 K, but they disappear at ST temperatures of 1123 and 1243 K. The numbers of both α phases decreases with increasing ST temperature. The numbers of both α phases with relatively high aspect ratios increases with increasing ST temperature.

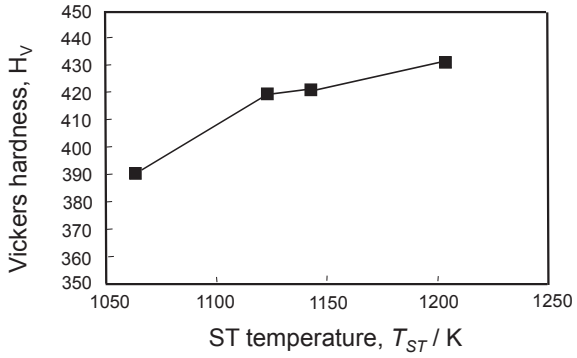

Fig. 8 Vickers hardness values of ST/1063 K, ST/1123 K, ST/1143 K, and ST/1203 K as a function of ST temperature.

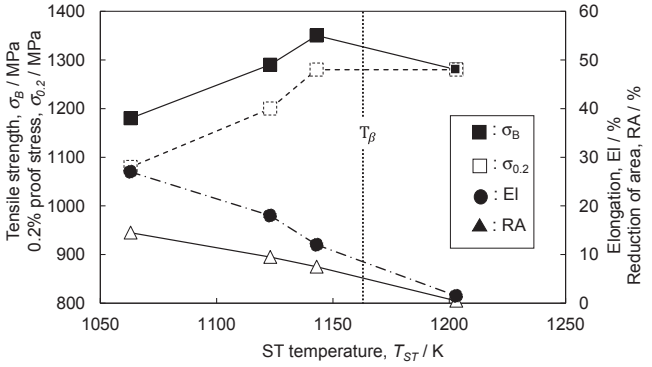

Fig. 9 Tensile properties of ST/1063 K, ST/1123 K, ST/1143 K, and ST/1203 K as a function of ST temperature.

3.2 Vickers hardness

Vickers hardness values of ST/1063 K, ST/1123 K, ST/1143 K, and ST/1203 K are shown in Fig. 8 as a function of ST temperature. The Vickers hardness increases with increasing ST temperature.

3.3 Tensile properties

The tensile properties as a function of ST temperature and stress-strain curves of ST/1063 K, ST/1123 K, ST/1143 K, and ST/1203 K are shown in Figs. 9 and 10. Notably, the 0.2% proof stress, $\sigma_{0.2}$, and tensile strength, σ_B, increase with increasing ST temperature up to 1143 K within the $(\alpha + \beta)$ region, but decrease with further increasing ST temperature to 1203 K within the β region. In addition, the elongation, EL, and reduction of area, RA, decrease with increasing ST temperature and becomes nearly 0%, corresponding to an ST temperature of 1203 K. Interestingly, the $\sigma_{0.2}$ and σ_B of ST/1203 K are equivalent. The specimen is likely fractured in elastic deformation region of true stress-strain curve, which will be shown below. However, $\sigma_{0.2}$ was obtained in ST/1203 K as stated above. Therefore, a small amount of plastic deformation seems to be occurred, but ST/1203 K is fractured in a brittle manner.

SEM fractographs of ST/1063 K, ST/1123 K, ST/1143 K, and ST/1203 K are shown in Fig. 11. Ductile transgranular fracture morphologies are observed in the fracture surfaces of

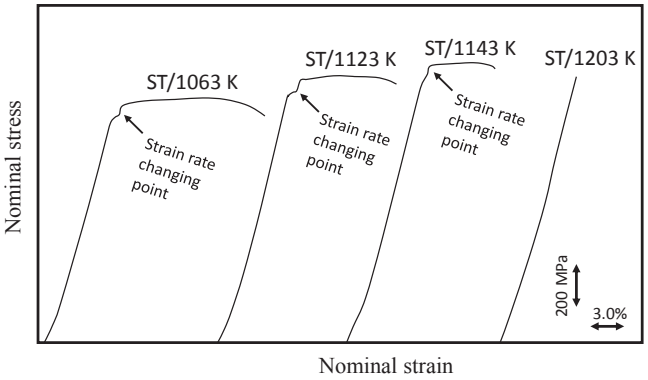

Fig. 10 Tensile stress-strain curves of ST/1063 K, ST/1123 K, ST/1143 K, and ST/1203 K.

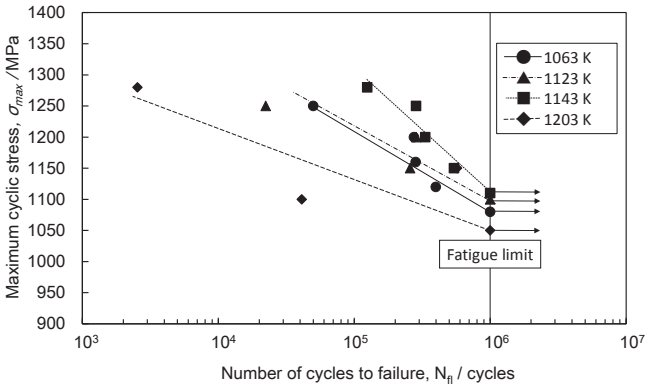

Fig. 12 Fatigue lives under load-controlled conditions of ST/1063 K, ST/1123 K, ST/1143 K, and ST/1203 K as maximum cyclic stress (σ_{max})-number of cycles to failure (N_{fl}) (S-N_{fl}) curves.

ST/1063 K, ST/1123 K, and ST/1143 K, although the fracture surface becomes flatter and the depth of dimples becomes shallower with increasing ST temperature. However, a brittle grain boundary fracture is observed in the fracture surface of ST/1203 K, because the intragrain strength exceeds the strength of the prior β grain boundary due to the precipitation of secondary α by aging treatment.

The tensile stress-strain curves of ST/1063 K, ST/1123 K, ST/1143 K, and ST/1203 K well exhibits the their fracture trends as described above.

3.4 Fatigue life under load-controlled conditions: high cycle fatigue life

Fatigue lives under load-controlled conditions of ST/1063 K, ST/1123 K, ST/1143 K, and ST/1203 K are shown in Fig. 12 as maximum cyclic stress, σ_{max}, -number of cycles to failure, N_{fl}, (S-N_{fl}) curves. The fatigue limit increases with increasing ST temperature up to 1143 K, corresponding to the $(\alpha + \beta)$ region; however, it decreases with further increase in the ST temperature to 1203 K. Accordingly, ST/1203 K exhibits the lowest fatigue limit.

SEM fractographs of ST/1063 K, ST/1123 K, ST/1143 K, and ST/1203 K subjected to the load-controlled fatigue tests are shown in Fig. 13. The crack initiates from the surface of the specimen for ST/1203. The crack initiation site is featureless and the crack propagation region exhibits a brittle fracture surface showing grain boundary fracture morphology similar to that of its tensile fracture surface. However, the crack initiates from subsurface of the specimen for ST/1063 K, ST/1123 K, and ST/1143 K: the subsurface crack initiation site was observed in 80% of the specimens.

The differences in the fracture surface and microstructural morphologies, and fatigue strength and tensile properties of ST/1203 K, which is subjected to ST in the β region, from those of ST/1063 K, ST/1123 K, and ST/1143 K, which are subjected to ST in the $(\alpha + \beta)$ region are relatively large, and Ti-17 subjected to ST in the β region is not suitable for practical applications in engine components. Furthermore, the fatigue ratio demonstrates more clearly the resistance to fatigue failure of materials because fatigue failure is caused at very restricted weak site in the microstructure such as α phase

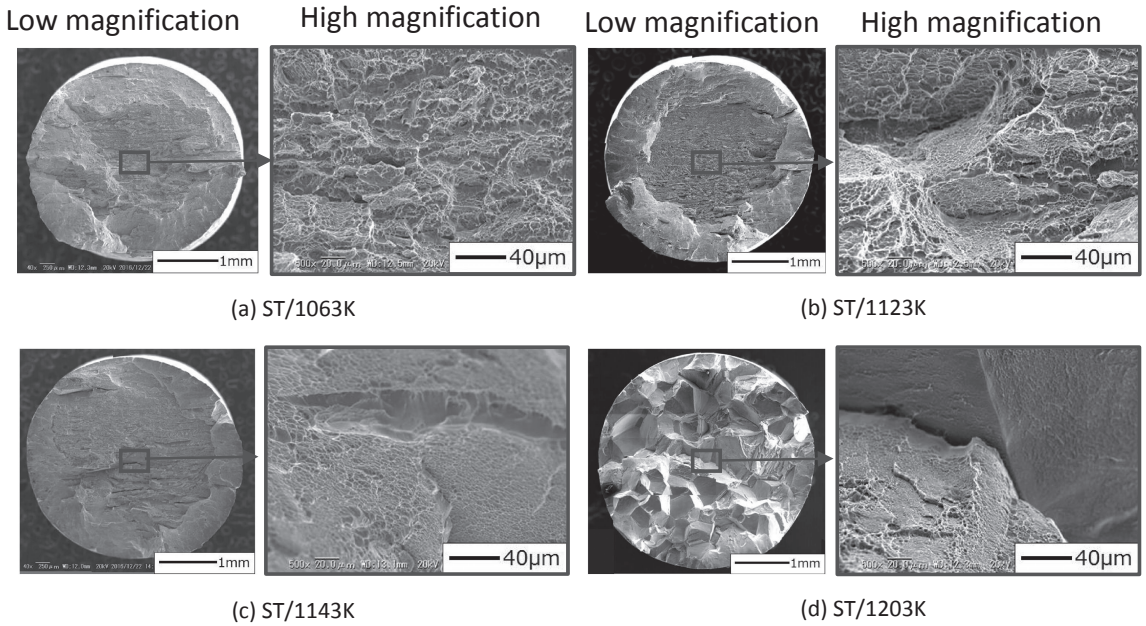

Fig. 11 Low and highly magnified SEM fractographs of ST/1063 K, ST/1123 K, ST/1143 K, and ST/1203 K subjected to tensile tests.

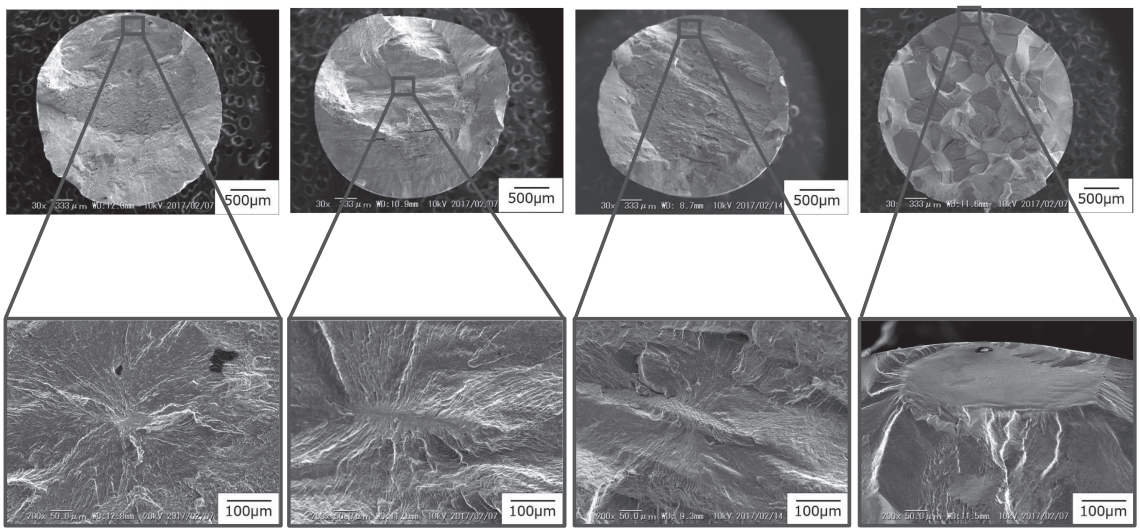

(a) ST/1063 K (b) ST/1123 K (c) ST/1143 K (d) ST/1203 K

Fig. 13 SEM fractgraphs of ST/1063 K, ST/1123 K, ST/1143 K (upper side), and their crack initiation sites (bottom side) subjected to load-controlled fatigue tests.

and interface between α and β phases as compared with the case of tensile fracture. The fatigue cracks of the ($\alpha + \beta$)-type titanium alloys such as Ti–6Al–4V, Ti–6Al–7Nb, and Ti-17 subjected to aging treatment after solution treatment below β transus temperature having primary α phase were reported to initiate at slip band formed in primary α phase,[8,9] micro crack formed at interface between primary α and β phases,[8] interface of primary α phase,[10,11] or interface between primary α phase and (β + secondary α phase)-region.[9–11] On the other hand, in the ($\alpha + \beta$)-type titanium alloys such as Ti–6Al–4V and Ti–6Al–7Nb subjected to aging treatment after solution treatment over β transus temperature having acicular α phase in the whole microstructure, the fatigue cracks were reported to initiate in unit of colony or prior β grain.[9–11] The fatigue crack initiation mechanism is different between the alloys having primary α phase and acicular α phase in the whole microstructure. The morphologies of the fatigue surfaces of ST/1063 K, ST/1123 K, and ST/1143 K are similar each other, but significantly different from that of ST/1203 K in this study. Therefore, the fatigue ratios (maximum cyclic stress range at each number of cycles to failure/tensile strength) of ST/1063 K, ST/1123 K, and ST/1143 K having primary α phases are shown in Fig. 14 as a function of the number of cycles to failure. The fatigue ratios at the fatigue limits of ST/1063 K, ST/1123 K, and ST/1143 K are 0.92, 0.85, and 0.82, respectively. Therefore, ST/1063 K shows the greatest fatigue ratio at the fatigue limit, which was shown in Fig. 14.

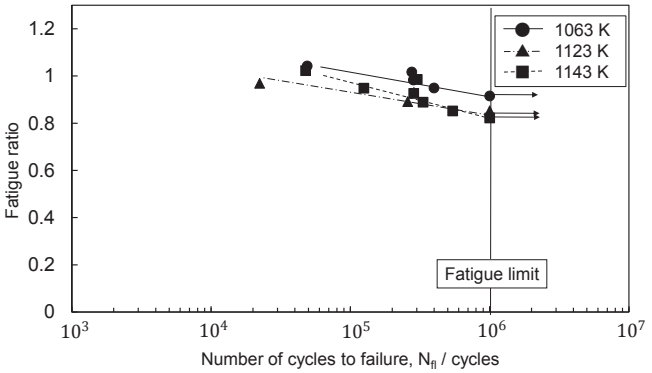

Fig. 14 Fatigue ratios under load-controlled conditions of ST/1063, ST/1123, and ST/1143 as a function of number of cycles to failure.

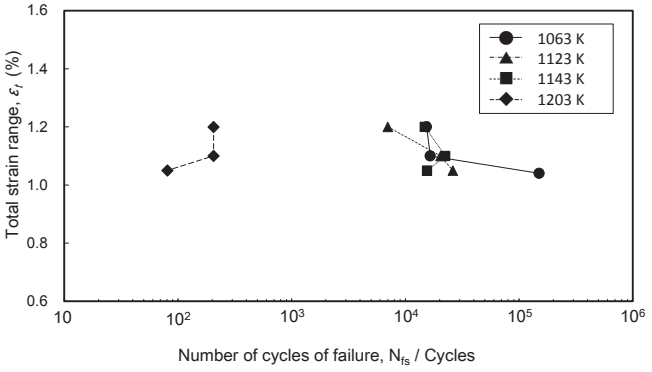

Fig. 15 Fatigue lives of ST/1063 K, ST/1123 K, ST/1143 K, and ST/1203 K under strain-controlled conditions as total strain range (ε_t)-number of cycles to failure (N_{fs}).

3.5 Fatigue life under strain-controlled conditions: low cycle fatigue life

Fatigue lives of ST/1063 K, ST/1123 K, ST/1143 K, and ST/1203 K under strain-controlled conditions are shown in Fig. 15 as the total strain range, $\Delta\varepsilon_t$, as a function of number of cycles to failure, N_{fs}. The fatigue life tends to increase with decreasing ST temperature and $\Delta\varepsilon_t$ in the case of ST/1063 K, ST/1123 K, and ST/1143 K contrary to the trend recognized in the fatigue life under load-controlled conditions. A.W. Funkenbusch and L.F. Coffin[6] have reported the low cycle fatigue life of Ti-17 fabricated under nearly the same condition as that of present ST/1063 K, and its reported fatigue life is nearly the same as that of the present ST/1063 K.

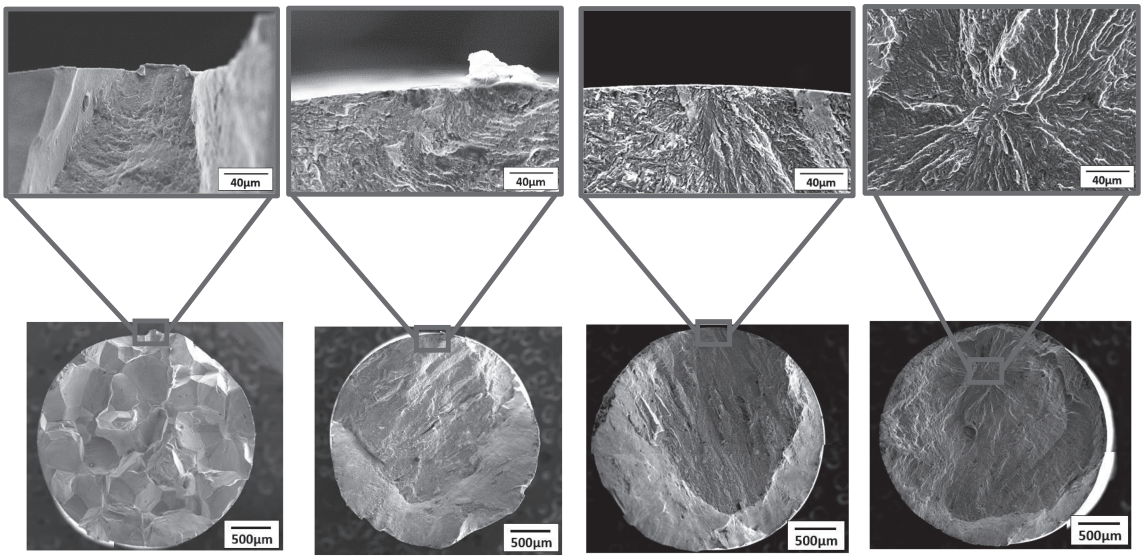

(a) ST/1203K (b) ST/1143K (c) ST/1123K (d) ST/1063K

Fig. 16 SEM fractographs of (a) ST/1203 K, (b) ST/1143 K, (c) ST/1123 K, and (d) ST/1063 K subjected to strain-controlled fatigue tests at a total strain range, $\Delta\varepsilon_\tau = 1.05\%$ (bottom side) and their crack initiation sites (upper side).

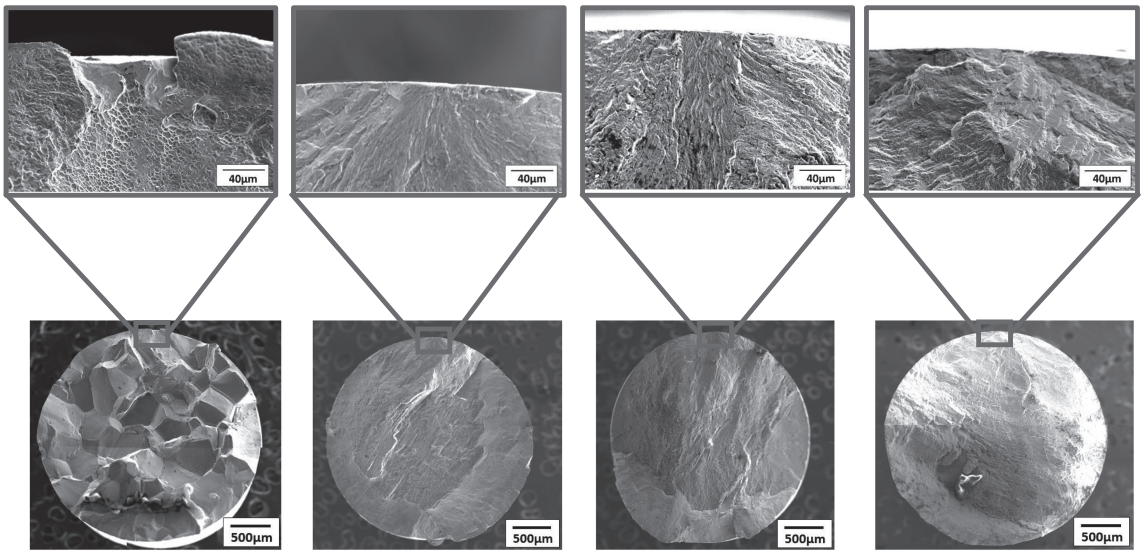

(a) ST/1203K (b) ST/1143K (c) ST/1123K (d) ST/1063K

Fig. 17 SEM fractographs of (a) ST/1203 K, (b) ST/1143 K, (c) ST/1123 K, and (d) ST/1063 K subjected to strain-controlled fatigue tests at a total strain range, $\Delta\varepsilon_t = 1.2\%$ (bottom side) and their crack initiation sites (upper side).

The fatigue life is the worst in the case of AT/1203 K; this trend is same as that in its fatigue life under load-controlled conditions. The fatigue life of AT/1203 K is, in particular, not well related to $\Delta\varepsilon_t$; this seems to be related to the brittleness of this material.

Although there maybe possibility to get better correlation between the plastic strain range or elastic strain range and the number of the cycles to failure, the total strain range, $\Delta\varepsilon_t$, is used to relate with the fatigue life, namely the number of cycles to failure in this study. Further investigation is required to make this problem to be clear in future.

SEM fractographs of ST/1063 K, ST/1123 K, ST/1143 K, and ST/1203 K subjected to strain-controlled fatigue tests at total strain ranges of 1.05% and 1.2% are shown in Figs. 16 and 17. Almost all of the cracks tend to initiate from the surface of the specimen although almost all the cracks tend to initiate from the subsurface of the specimen under load-controlled conditions as stated above. The difference in the fatigue crack initiation site between load- and strain-controlled conditions are currently unclear. Further investigations are necessary to solve this problem in future.

3.6 Quantitative relationship of fatigue life and microstructural factor or tensile property

(1) Under load-controlled conditions

The authors focused on the samples subjected to solution treatment at temperatures less than the β transus temperature according to the discussion on the crack initiation mechanism stated above in the section of 3.4. The relationship between the fatigue ratio at fatigue limit, R, and the volume fraction of

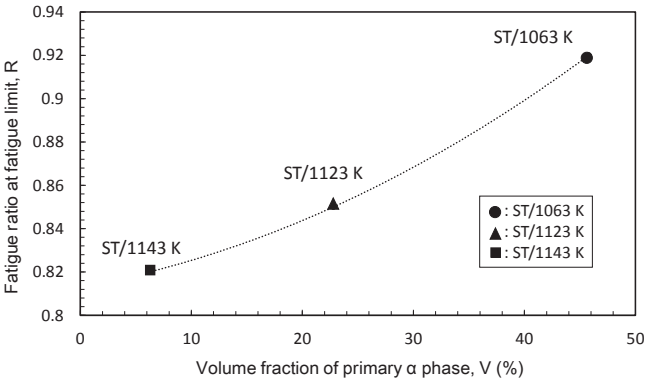

Fig. 18 Relationship between fatigue ratio, R, under load-controlled conditions and volume fraction of primary α phase.

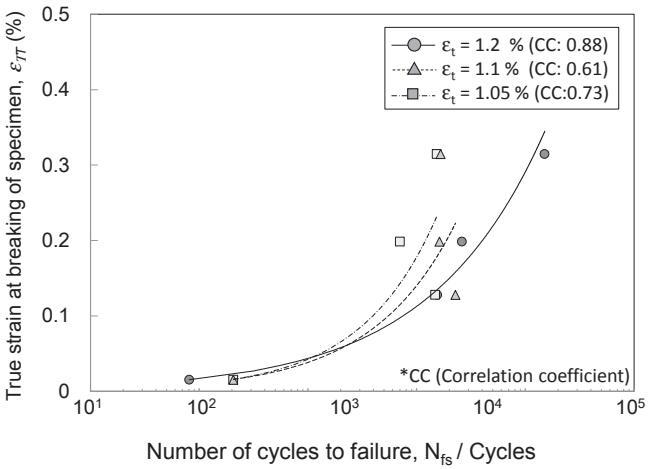

Fig. 19 Relationship between the tensile true strain, ε_{TT}, at breaking of specimen obtained by tensile test and fatigue life under strain-controlled conditions, which is the number of cycles to failure, N_{fs}, for each total strain range.

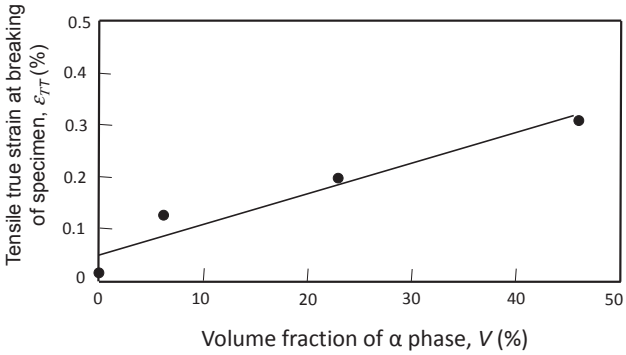

Fig. 20 Relationship between the tensile true strain, ε_{TT}, at breaking of specimen obtained by tensile test and volume fraction of primary α phase, V(%).

the primary α phase, V(%), for the samples subjected to ST at temperatures less than the β transus temperature was found as shown in Fig. 18 in this study: the volume fraction of the primary α phase is inversely related to that of the secondary α phase. This relationship can be expressed as the following equation.

$$R = F_l/\sigma_B = 0.80e^{0.0029V(\%)} \quad (1)$$

where F_l and σ_B are the fatigue limit and the tensile strength, respectively.

Therefore, the fatigue limit can be calculated using eq. (1) when the tensile strength and volume fraction of the primary α phase are known. However, the accuracy of the eq. (1) should be more raised by increasing the data points in future.

(2) Under strain-controlled conditions

The fatigue life, which is the number of cycles to failure, N_{fs}, for each $\Delta\varepsilon_t$ was found to be well related to the tensile ductility, namely elongation obtained by tensile testing sated above. Therefore, the tensile true strain at breaking of the specimen, ε_{TT}, which is well express the tensile ductility was adopted to relate with N_{fs}. The relationship between ε_{TT} and N_{fs} for each $\Delta\varepsilon_t$ is shown in Fig. 19. ε_{TT} was calculated by the following equation.

$$\varepsilon_{TT} = \ln(A_I/(A_I - A_F)) \quad (2)$$

where A_I and A_F are the initial cross section of the tensile specimen and the cross section of the fractured tensile specimen, respectively.

The relationship between ε_{TT} and N_{fs} for each total strain range, $\Delta\varepsilon_t = 1.05$, 1.10, or 1.2% can be expressed by the following equations.

$$\varepsilon_{TT} = 0.6 \cdot 10^{-3} N_{fs}^{0.62} \quad \text{for } \Delta\varepsilon_t = 1.05\% \quad (3)$$

$$\varepsilon_{TT} = 0.8 \cdot 10^{-3} N_{fs}^{0.56} \quad \text{for } \Delta\varepsilon_t = 1.10\% \quad (4)$$

$$\varepsilon_{TT} = 2.5 \cdot 10^{-3} N_{fs}^{0.41} \quad \text{for } \Delta\varepsilon_t = 1.2\% \quad (5)$$

Therefore, the low cycle fatigue life is well quantitatively related to the ductility of the materials in this study.

ε_{TT} was also found to be well linearly related to V(%) of the primary α phase as show in Fig. 20. ε_{TT} can be expressed by the following equation.

$$\varepsilon_{TT} = 5.9 \times 10^{-3} \cdot V(\%) + 5.3 \times 10^{-2} \quad (6)$$

Therefore, quantitative relationship between the fatigue life (the number of cycles to failure: N_{sf}) for each ε_t and V(%) can be given by following each equation.

$$N_{fs} = e^{1.6\log(9.8\cdot V(\%)+88.3)} \quad \text{for } \Delta\varepsilon_t = 1.05\% \quad (7)$$

$$N_{fs} = e^{1.8\log(7.4\cdot V(\%)+66.3)} \quad \text{for } \Delta\varepsilon_t = 1.1\% \quad (8)$$

$$N_{fs} = e^{2.4\log(2.4\cdot V(\%)+21.2)} \quad \text{for } \Delta\varepsilon_t = 1.2\% \quad (9)$$

The fatigue live under strain-controlled conditions for each total strain range is swell quantitatively related to the volume fraction of the primary α phase.

4. Conclusions

The fatigue lives of forged Ti-17 subjected to different solution treatments and a common aging treatment (ST/1063 K, ST/1123 K, ST/1143 K, and ST/1203 K) were evaluated under load- and strain-controlled conditions for high and low cycle fatigue lives, respectively. Then, the relationships between fatigue lives and microstructural factors were examined quantitatively and qualitatively. The following results were obtained in this study.

(1) The microstructure of the forged Ti-17 subjected to solution treatment at 1203 K, which is more than the β transus temperature, and aging treatment exhibits

equiaxed prior β grains composed of fine acicular α. However, the microstructures of the forged Ti-17 subjected to solution treatment temperatures at 1063 K, 1123 K, and 1143 K, which are less than the β transus temperature, and aging treatment exhibit elongated prior β grains composed of two different microstructural feature regions, which are acicular and fine spheroidal α phase regions. The width of the prior β grain of the forged Ti-17 subjected to solution treatment less than the β transus temperature, increases with increasing solution treatment temperature.

(2) The Vickers hardness of the forged Ti-17 subjected to solution and aging treatments increases with increasing solution treatment temperature.

(3) The 0.2% proof stress and tensile strength of the forged Ti-17 subjected to solution and aging treatments increase with increasing solution treatment temperature up to 1143 K within the $(\alpha + \beta)$ region, but decrease with further increasing solution treatment temperature to 1203 K within β region. The elongation and reduction of area decrease with increasing solution treatment temperature, and it becomes nearly 0% corresponding to a solution treatment temperature of 1203 K.

(4) The high cycle fatigue limit increases with increasing solution treatment temperature up to 1143 K, corresponding to the $(\alpha + \beta)$ region. However, it decreases with further increase in the solution treatment temperature to 1203 K in the β region.

(5) The high cycle fatigue ratio at fatigue limit increases with decreasing solution treatment temperature, namely increasing volume fraction of the primary α phase, and relates well qualitatively with the volume fraction of the primary α phase when the solution treatment temperature is less than the β transus temperature.

(6) The low cycle fatigue life increases with decreasing solution treatment temperature, namely increasing the volume fraction of the primary α phase.

(7) The low cycle fatigue life relates well quantitatively with the tensile true strain and the volume fraction of the primary α phase for each total strain range.

Acknowledgement

This work was partly supported by the Structural Materials for Innovation, Cross-ministerial Strategic Innovation Promotion Program, Cabinet Office, Government of Japan.

REFERENCES

1) I. Inagaki, T. Takechi, Y. Shirai and N. Ariyasu: Nippon Steel & Sumitomo Metal Technical Report **106** (2014) 22–27.
2) T.K. Redden: *Beta Titanium Alloys in the 1980's*, ed. by R.R. Boyer and H.W. Rosenberg, (AIME, Warrendale, PA, USA, 1984) pp. 239–254.
3) Titanium alloys, *Materials Properties Hand Book*, ed. by R. Boyer, G. Weisch and E.W. Collings, (ASM Int., Materials Park, OH, USA, 1994) pp. 453–463.
4) J. Xu, W. Zeng, Z. Jia, X. Sun and J. Zhou: J. Alloys Compd. **618** (2015) 343–348.
5) M.A. Moshier, T. Nicholas and B.M. Hillberry: Int. J. Fatigue **23** (2001) S253–S258.
6) A.W. Funkenbusch and L.F. Coffin: Metall. Trans. A **9** (1978) 1159–1167.
7) Y. Yamabe-Mitarai: Bull. Iron and Steel Inst. (Ferrum) **22** (2017) 480–486.
8) K. Minakawa: Tetsu-to-Hagané **75** (1989) 1104–1110.
9) J.A. Hall: Int. J. Fatigue **19** (1997) S23–S37.
10) T. Akahori, M. Niinomi and K. Fukunaga: Metall. Mater. Trans. A **31** (2000) 1937–1948.
11) T. Akahori, M. Niinomi, K. Fukunaga and I. Inagaki: Metall. Mater. Trans. A **31** (2000) 1949–1958.